Lab on a Chip

Distal modulation of bacterial cell-cell signalling in a synthetic ecosystem using partitioned microfluidics

Journal:	*Lab on a Chip*
Manuscript ID:	LC-ART-01-2015-000107
Article Type:	Paper
Date Submitted by the Author:	28-Jan-2015

Complete List of Authors:	Luo, Xiaolong; Catholic University, Mechanical Engineering Tsao, Chen-Yu; University of Maryland, Institute for Bioscience and Biotechnology Research (IBBR) Wu, Hsuan-Chen; University of Maryland, Institute for Bioscience and Biotechnology Research (IBBR) Quan, David; University of Maryland, Fischell Department of Bioengineering; University of Maryland, Institute for Bioscience and Biotechnology Research (IBBR) Payne, Gregory; University of Maryland, Institute for Bioscience and Biotechnology Research Rubloff, Gary; University of Maryland, Materials Science and Engineering Bentley, William; University of Maryland, Fischell Department of Bioengineering

Cite this: DOI: 10.1039/c0xx00000x

www.rsc.org/xxxxxx

ARTICLE TYPE

Distal modulation of bacterial cell-cell signalling in a synthetic ecosystem using partitioned microfluidics

Xiaolong Luo,[a] Chen-Yu Tsao,[b] Hsuan-Chen Wu,[b] David N. Quan,[b,c] Gregory F. Payne,[b,c] Gary W. Rubloff[d,e] and William E. Bentley*[b,c]

Received (in XXX, XXX) Xth XXXXXXXXX 20XX, Accepted Xth XXXXXXXXX 20XX
DOI: 10.1039/b000000x

The human gut is over a meter in length, liquid residence times span several hours. Recapitulating the human gut microbiome "on chip" holds promise to revolutionize therapeutic strategies for a variety of diseases, as well as for maintaining homeostasis in healthy individuals. A more refined understanding of bacterial-bacterial and bacterial-epithelial cell signalling is envisioned and such a device is a key enabler. Indeed, significant advances in the study of bacterial cell-cell signalling have been reported, including at length and time scales of the cells and their responses. Few reports exist, however, where signalling events that span physiologically relevant time scales are monitored and coordinated. Here, we employ principles of biofabrication to assemble, *in situ,* cell communities that are (i) spatially adjacent within partitioned microchannels for studying near communication and (ii) distally connected within longitudinal microfluidic networks so as to mimic long distance signalling among intestinal flora. We observed native signalling processes of the bacterial quorum sensing autoinducer-2 (AI-2) system among and between these communities. Cells in an upstream device successfully self-reported their activities and also secreted autoinducers that were carried downstream to the assembled networks of bacteria that reported on their presence. Furthermore, active signal modulation of among distal populations was demonstrated in a "programmed" manner where "enhancer" and "reducer" communities were assembled adjacent to the test population or "reporter" cells. The modulator cells either amplified or attenuated the cell-cell signalling between the distal, already communicating cell populations. Modulation was quantified with a bioassay, and the reaction rates of signal production and consumption were further characterized using a first principles mathematical model. Simulated distribution profiles of signalling molecules in the cell-gel composites agreed well with the observed cellular responses. We believe this simple platform and the ease by which it is assembled can be applied to other cell-cell interaction studies among various species or kingdoms of cells within well-regulated microenvironments.

Introduction

Molecular signalling serves to coordinate biological function among individual cells, collections of cells (e.g., quorum sensing within bacterial populations), and within cell collections such as those in tissues. The human gut microbiome consists of all these cell systems where an open molecular "dialogue" maintains normal function. That is, bacterial signalling molecules secreted by commensal microorganisms and released into the gastrointestinal (GI) tract are transported both radially among commensal flora and epithelial cells within the lamina propria and longitudinally through the stomach, duodenum, jejunum, ileum (small intestine), and colon (large intestine). Cellular crosstalk enabled through these molecular species helps to maintain homeostasis by constant surveillance and regulation of the symbiotic relationships within the microbiome and between the microbiome and the host[1-4]. For example, the complex microbiota of the GI tract facilitates food breakdown, nutrient uptake, vitamin production, among other functions while at the same time provides a means to prevent pathogen outgrowth of commensal strains[5, 6]. On the other hand, a number of diseases such as inflammatory bowel diseases (IBD)[7], Gauchey's, Crohns, and even obesity[4, 8] have been correlated with a dysbiosed microbiota[9, 10].

Because of its relevance and the difficulty in accessing these molecular communication networks within humans and animals, the human intestinal microbiota composition and signalling activity have been the focus of new microsystems technologies[5-10]. For example, researchers are developing whole cell sensing systems to monitor quorum sensing molecules over the course of time to elucidate the bacterial load, extent of inflammation and progress of disease[11, 12] by evaluating the presence of distinct concentrations of quorum sensing molecules in saliva and stool samples. To better understand the population dynamics and cell-cell signalling interactions of the intestinal microbiome, *in vitro* platforms are needed which (1) enable confinement of the various cells with spatially controlled 3D microenvironments, and (2)

reflect the length and time scales of signalling molecules and cells in the natural systems. Recently, significant advances have been made towards the establishment of *in vitro* models to study bacterial communications with spatial control in synthetic microenvironments[13-17]. Few reports exist, however, where signalling events that span physiologically relevant time scales are coordinated and monitored. Here we elaborate on a system that investigates the interaction among distally connected cell populations that mimic the time scale of small molecule signalling events in human GI, and further exemplify the intricate signalling modulations in human GI microbiome using a simplified *in vitro* platform in a spatiotemporally controlled manner.

Recently, we introduced "biofabrication" as a means to rapidly and with minimal instrumentation, construct stratified biofilm mimics in fluidic systems. We demonstrated direct observation and manipulation of bacterial cell-cell signalling inside cell-gel composites[18-20]. In particular, we showed that liquid flow dynamics play a key role in manipulating the signalling events among individual cells that are proximally located inside the synthetic microenvironments. Then, recapitulation of the native system will also require that the interrogation of molecular signalling should be possible among distal populations, as remote signalling is likely to be altered by the presence of modulating cells located in between.

Specifically in this report, we demonstrate a synthetic ecosystem within a partitioned and longitudinal microfluidic model that modulates communication between distally located cells, with a transmission/detection gap of ~2 hrs (Fig. 1), a time period employed for *in vitro* human digestion models[21]. Signal molecule autoinducer-2 (AI-2) that is secreted from a transmitter cell community was transported by flow on the time scale of hours to a downstream ecosystem where cellular responses were modulated and biologically recorded. That is, the downstream community consisted of two distinct subpopulations, the first a "modulator" population, which either amplified or attenuated the flux of the signalling molecules forwarded to the second "reporter" subpopulation. In this way, cell signalling events are recorded in near real time and *in situ* by the incorporation of an adjacent engineered sensor strain. The combination of simply and rapidly-assembled cell populations connected via longitudinal microfluidic networks and the incorporation of sensing modalities *in situ* will enable more comprehensive analysis of on-chip human gut microbiome systems.

Materials and methods

Chitosan solution of 0.5% w/v, pH 5 was prepared by dissolving chitosan flakes (Sigma Aldrich, 85% deacetylated, medium molecular weight) in de-ionized water, with HCl added drop-wise to pH ~ 2 and left overnight, followed by drop-wise addition of 1 M NaOH to adjust the final pH to 5[22]. Alginate solution of 1% w/v, pH 7 was prepared by dissolving sodium alginate powder (Sigma Aldrich, medium viscosity) in distilled water, followed by stirring on stirring plate overnight. FluoSpheres (amine-modified nanospheres, Invitrogen, 200 nm, F-8764) were used to fluorescently decorate alginate. A 5 nL FluoSpheres solution was diluted 1000 times and mixed with 5 mL alginate solution (0.5% w/v), and used to evaluate flow patterns (Supplemental).

A. Device fabrication

Microfluidic devices were fabricated via soft lithography. Briefly, a mold with microchannel patterns was microfabricated on a 4" silicon wafer with negative photo resist SU-8 50. Sylgard 184 and curing agent (Dow Corning) were mixed at a 10:1 ratio, degassed and cured on the SU-8 mold in a 65°C oven for two hours. The cured PDMS of ~ 3 mm in thickness were then delaminated from the mold, punched with input/output holes using a Harris Uni-core punch (Ted Pella Inc, 1.0 mm), and then permanently bonded to piranha-cleaned 1" x 3" glass slides by oxygen plasma treatment using a March Jupiter III machine. The final microchannels were 1 mm wide and 235 ± 15 µm high with the middle joint area of 3 mm wide, as shown in Fig. 1(b).

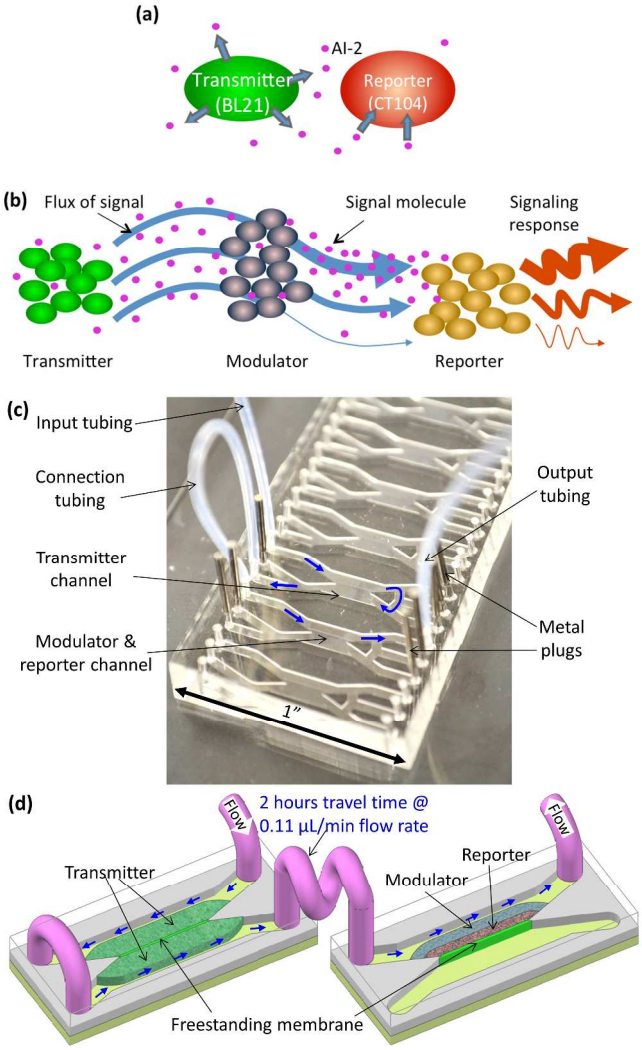

Fig. 1 Microfluidic system for enabling and manipulating of bacterial cell-cell communication among proximal cells and between distant populations **(a)** Model of cell-cell signalling or quorum sensing (QS) (b) Flux of signal molecules from transmitter to reporter is either enhanced or reduced by modulating cells. **(c)** A device with multiple microchannels, two of which were sequentially connected via flexible tubing for signaling experiments. Flow patterns are indicated with blue arrows. **(d)** Schematic of spatially localized and *in situ* assembled cell-gel composites within two connected microchannel systems; the blue arrows indicate the direction of the flow. Note that the bright green chitosan membrane is assembled prior to cell-gel composites.

B. Membrane formation and cell-gel assembly

A simple pumping strategy that employs air plugs of 0.3 ~ 2 mL as damping reservoirs in syringes were enlisted to achieve stable flow interfaces and pH gradients in microchannels. A previously reported self-balancing mechanism was employed to ensure reliable biofabrication[23]. Freestanding chitosan membranes were first fabricated with fluidically generated pH gradients at the interface of two adjacent flow streams[23] and these partitioned a converging microchannel into two while allowing diffusion of small molecules between microchannel compartments. The chitosan membrane also serves as a scaffold for the subsequent assembly of various cell populations as described below.

That is, calcium alginate hydrogels are formed that place cells-of-interest directly adjacent to the previously assembled chitosan membranes[19]. Briefly, solutions of target cells were mixed in alginate solution and converted into a cell-gel composite along the chitosan membrane by the complexation with Ca^{2+}. This was enabled by calcium ions (4mM calcium chloride, pH 7) present in the channel on the opposite side diffusing through the chitosan membrane and complexing with cells and alginate on the proximal side[19]. In this study, cells in exponential growth phase ($OD_{600} \approx 0.8$) were spun down and mixed with 1% (w/v) alginate solution and adjusted with Luria-Bertani (LB) medium to final cell density of 1.5 OD cells and 0.5% (w/v) alginate. After the desired thickness of cell-gel composite was formed (by visual inspection), the microchannel was rinsed with DI water and was therefore ready for the assembly of a next layer of cell-gel composite.

In order to ensure significant signal molecule generation, transmitter cells were assembled into two calcium alginate hydrogels sandwiching a freestanding chitosan membrane in an upstream channel. The flow output of one side was fluidically connected to the other side of the sandwich cell-gel composites, as shown in the scheme of Fig. 1(d). Therefore, the AI-2 level in the flow leaving the upstream transmitter cells was the integrated output from the two cell-gel composites. The reporter and modulator cells were assembled in calcium alginate hydrogels in a downstream channel (Fig. 1(d)). For the control experiments, clear hydrogel, instead of modulator cells, was assembled as an outer layer adjacent to the inner reporter cell-gel layer.

The two microchannels were remotely connected with PTFE tubing that was 10 cm long to mimic the signal transport in intestinal flora. As a result, it took ~2 hours for a flow of 0.11 μL/min to transport small molecules from the upstream channel to the downstream channel. All bright field optical images and fluorescent images of cell-gel assembly were obtained with a 10X objective under a Carl Zeiss LSM-310 microscope.

C. Bacterial stains and cell-cell signalling studies

The *E. coli* bacterial strains and plasmids used in this study are listed in Table 1. Cells were grown in LB medium supplemented with kanamycin (50 μg/mL) and/or ampicillin (50 μg/mL) according to their antibiotic resistance profiles (Sigma Aldrich) at 37°C with shaking (250 rpm) for overnight to OD_{600} of 3.4 ~ 4.5 (w/slight batch to batch variation) before being assembled. Cell signalling studies were performed in a humidified environmental chamber (Precision Plastics, MD) at 37°C. Neither the generation of air bubbles nor evaporation were found to be an issue. Assembled cells in devices were cultured with LB medium supplemented with kanamycin (50 μg/mL) to prevent cross contamination. Also, calcium chloride was added (1 mM) to maintain integrity of the cell-gel composites throughout. The culturing solution was introduced into the microchannels at 0.11 μL/min flow rate, the slowest flow rate of the Genie syringe pumps (Kent Scientific, CT). The cell responses were monitored with an inverted fluorescent microscope (Nikon ECLIPSE TE2000). Fluorescence images of cell response to AI-2 (expression of fluorescent proteins) were obtained with a 20X objective under the Nikon microscope. The bright field optical microscopic images were obtained with transmitted incandescent light. Bright field images showed that the alginate hydrogels stayed intact. We did not find cell leakage from the alginate hydrogels during the first 12 hours, however, shortly thereafter cells were observed to out grow their hydrogel microenvironments, as they were observed outside the gels and within the microchannels. The cell responses were found to be stabilized after the first 10 hours, as evidenced by the plateau status of the responsive curves in Fig. 6. This suggests no significant effect resulting from the cell outgrowth after the initial 12 hours. The fluorescence microscope images were obtained with FITC or TRITC filter sets. Images were processed with ImageJ.

Table 1. Bacterial strains used in this study

Stains	*Plasmid Transformed*	*Properties*
Transmitter BL21	pCT5 + pET200-GFPuv	Produce AI-2 and express GFP constitutively[24].
Reporter CT104 W3110 (*lsrFG-luxS-*)	pCT6 pET200-DsRed	Sense AI-2 by expressing DsRed; higher sensitivity due to deletion of *lsrFG*[25].
Enhancer LW5 W3110 (*lsrACDBFG*)::kan		Produce AI-2 but without AI-2 *lsrACDB* transporters[26]
Reducer LW8 ZK126 (*lsrR*)::kan		Produce AI-2 and consume large amounts of AI-2 due to lack of repressor, LsrR[26]

D. AI-2 activity assay and numeric modelling

As shown in Fig. 2(a), effluent solutions after the transmitter cells in the upstream channel were either collected directly as (1) controls for independent bioassays, or they were transported through the downstream channels that contained one of the three test populations: (2) test strain and reporter CT104, (3) enhancer LW5, or (4) reducer LW8. The effluent solutions were collected for 18 hours, with the sampling tubes maintained in an ice bath. The collected samples were centrifuged, and the cell-free solution was extracted and frozen in - 20°C before being used for a *Vibrio harveyi* BB170 AI-2 bioassay, which was conducted as previously noted[27]. In brief, *V. harveyi* BB170 was grown for 16 h in autoinducer bioassay (AB) media and then diluted 5000 times in fresh AB media to obtain 10^5 CFU/ml. To test AI-2 in the cell-free sample solutions, 20 μL sample solution was added into 180 μL of the prepared cell solution and mixed thoroughly. For calibration purposes, 20 μL of AI-2 solution (prepared enzymatically *in vitro*[26]) of 1, 5, 10, 20 and 40 μM was also added into 180 μL of the prepared cell solution and mixed thoroughly. Two parallel tubes for each of the test samples and AI-2 control samples were prepared; all samples were incubated

in parallel at 30°C with agitation (250RPM). After 3 hours, bioluminescence was read every 30 min with a Luminoscan TL *plus* (ThermoLabsystems). The final reading of each condition was the average of the two parallel tubes with half of the tubes read in reverse order to control reading error.

Readings taken after 4.5 h of incubation were normalized to the positive control (case (1), sample collected directly after transmitter cells), as shown in Fig. S1(a). The relationship between the normalized AI-2 activities vs. concentrations of AI-2 control solutions is plotted in Fig. S1(b), which indicates a linear relationship for concentrations between 1 to 10 μM. AI-2 activity of the test samples in the cases of (1) control, (2) reporter, (3) enhancer and (4) reducer were then compared with the calibration curve in Fig. S1(b) and the AI-2 concentrations of the four samples were determined from within the linear range, as shown in Fig. 2(b).

To approximate AI-2 reaction rates, mathematical modelling of the AI-2 dynamics and distribution within the cell-gel composites and longitudinally through the two-stage fluidic system was performed using the multi-physics software COMSOL 4.3a. Geometry was created in AutoCAD 2012 (AutoDesk) and imported into COMSOL. A reaction flow in porous media model was used to represent the cell-gel composites. The diffusion coefficient of AI-2 molecules was assumed to be 0.75 x 10^{-9} m^2/s, similar to glucose in calcium alginate at 37°C[28]. The porosity of all the cell-gel composites was assumed to be 95%, similar to literature[29], and the permeability of which was assumed to be 10^{-9} cm^2, also taken from the literature[30]. The parameter sweeping strategy in COMSOL was applied to extract the reaction rates in the cell-gel composites based on the known input and output AI-2 concentrations. The simulation results were obtained directly from COMSOL, or were exported to Microsoft Excel for further processing.

Results and discussions

A. Experimental design to mimic transport in intestinal flora

We exploited biofabrication, a previously reported cell assembly strategy[19, 31], to mimic the longitudinal transport of small molecules transmitted by non-pathogenic *E. coli*, which are known to occupy the digestive tract, as shown in Fig.1. The signalling model employed in this study is the AI-2 quorum sensing system that is common among hundreds of bacterial strains[12, 32]. As shown in Fig. 1(a), the signal transmitter cells (BL21) simultaneously produced signal molecule AI-2 and constitutively expressed GFP for direct visualization. The reporting cells (CT104) lacked AI-2 production capability (*luxS*$^-$) but sensed AI-2 and subsequently expressed DsRed, which is an indicator of *lsr* gene expression (QS response)[24] and a proxy for many AI-2 regulated behaviours[25, 33, 34].

The transport of signalling molecules in microfluidics and the modulation of the signalling are schematically shown in Fig.1 (c) and (d), while Fig.1 (b) shows a device used for this study. The transmitter cells were assembled in an upstream ecosystem, and the reporter and enhancer/reducer cells (or clear gel in the case of control experiments) were assembled in a downstream ecosystem. The two microchannels were remotely connected via PTFE tubing (~10 cm long) to mimic the signal transport in intestinal flora, which imposes a 2-hour transport lag time for small molecules to move from the upper system to the lower system at a flow of 0.11 μL/min.

In addition to the flux of signal molecule AI-2 from transmitting cells to sensing cells, any other secreted molecules will transverse the device potentially modulating the reporter cells. In the case of the control (reporter cells), we expected a decrease in AI-2 level commensurate with its uptake from these *luxS*$^-$ cells. In addition, as noted above, we provided a third "modulator" cell population at the vicinity of the reporter cells. When the signal enhancer cells, LW5[26], were used as the modulator, a net increase in AI-2 was expected downstream as AI-2 was flowing to the modulator cells and was likely secreted by these same cells. When the signal consumer cells, LW8[26], were used as the modulator, we would expect most of the AI-2 to be consumed before it reached the reporter cells. The results for remotely transmitted signalling between the two connected (i.e., communicating) ecosystems and the effects of the third modulating population are explored in detail in the following sections.

B Modulation of communicating signal molecules AI-2 with engineered cell communities

Before investigating the modulation of the signalling between remotely connected cell populations, we performed AI-2 activity assays to estimate the amounts of AI-2 produced by the transmitter cell population and consumed by the reporter/modulator cells (Fig. 2(a)). The control (sample 1) refers to the effluent solution collected directly after it twice flowed past two conjoined layers of transmitter cells separated by a chitosan membrane within the same microchannel. The reporter (sample 2), enhancer (sample 3) and reducer (sample 4) refer to the effluent solutions collected after they flowed past one downstream cell-gel composite of either reporter cells, enhancer cells or reducer cells, respectively. The downstream ecosystem was connected with the upstream transmitter cell channel via a segment (10cm) of flexible PFTE tubing. This imposed a 2-hour delay for signalling molecules to be transported from the transmitting cells to the cells in the downstream channels. Samples were collected and AI-2 concentration was determined by BB170 assay[35]. By normalizing the AI-2 activity of the control sample, the activities of the reporter, enhancer and reducer were determined to be 0.62, 1.34 and 0.12, respectively (See Fig. S1(a)). AI-2 solutions of 1, 5, 10, 20 and 40 μM were added to LB media *in vitro* and similarly quantified using the BB170 assay to generate a calibration curve shown in Fig. S1(b). Based on this relationship between the calibration curve and the normalized AI-2 activity in Fig. S1, the AI-2 concentrations of all sample solutions were obtained. That is, we report the levels immediately following the (1) transmitter (control), (2) reporter, (3) enhancer and (4) reducer cells are 4.5, 3.0, 5.8 and 1.1 μM, respectively (Fig. 2(b)).

These results demonstrate that signalling molecules synthesized by transmitter cells were transported through the remotely connected downstream microchannels. Both the reporter and reducer cells consumed AI-2 in the flow, while the reducer cells were significant AI-2 consumers, taking in more AI-2 than the reporter cells. The enhancer cells produced additional

AI-2 and increased AI-2 concentrations in the flow. This confirms that the enhancer and reducer cells effectively modulated the signalling concentration between the transmitter cells and reporter cells. That is, these results demonstrate that signals from an upstream population serve to signal a distal population, which then modulates the downstream "ecosystem" in a defined and anticipated manner.

C. Simulated AI-2 synthesis rates of modulating cells

The effects of the enhancer, reporter and reducer cells on the signal molecules flowing past the cell-gel composites in the downstream microchannel were further investigated with numeric simulations. For this, we assumed unrestricted flow past the cell-gel composite and that the composite was a porous and permeable obstruction that had either reported, consumed or produced AI-2. With the estimated AI-2 input concentration of 4.5 µM and the estimated AI-2 output concentrations of 3.0, 5.8 or 1.07 µM shown in Fig. 3(a), we concluded that the reporter cell-gel composite was regarded as an AI-2 sink, the enhancer cell-gel composite was an AI-2 source, and the reducer cell-gel composite was regarded as a big AI-2 sink.

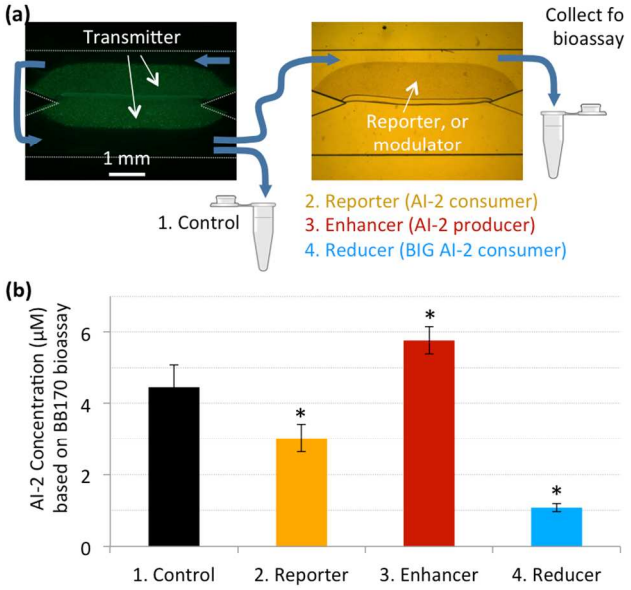

Fig. 2 Measurement of AI-2 activity in effluent solutions before and after being transported through the reporting or mediating cells. **(a)** Experimental configuration. **(b)** Calculated AI-2 concentration of effluent solutions for control and experiments, based on calibration curve of AI-2 activity with *in vitro* AI-2. The error bars represent the standard deviation of the BB17 bioassay. The * donates a statistical difference ($p < 0.05$ in all cases).

The velocity profiles of the flow passing and within the upstream transmitter cell-gel composites were simulated and shown in Fig. S2(a), while the velocity profiles of the flow passing and within the downstream modulator or reporter cell-gel composites was simulated and shown in Fig. 3(b). For this, we assumed a no-slip boundary condition and laminar flow into and out of the chamber. Our results show that fluid velocity in the unrestricted zones (~ 400 µm width) was ~ 25 µm/sec, while the fluid velocity in the same direction within the cell-gel composite (~ 1100 µm width) was less than 1 µm/sec. Hence, the majority (> 90%) of the fluid was found flowing past the cell-gel composites and only minimal flow penetrated into the hydrogels. This is consistent with experimental observation depicted in Fig. S3, where FITC-labelled nanospheres (200 nm in diameter) in alginate solution flowing pass the microchannel were seen as streamlines, while the nanospheres in the assembled alginate hydrogel were seen as clear fluorescent dots. The Péclet number, the ratio of advection over diffusion of AI-2 molecules in the cell-gel composite, was estimated to be about 0.8. Thus, both diffusion and convection processes contributed AI-2 to the downstream ecosystem. A parameter sweeping strategy in COMSOL was applied to extract the reaction rates in the upstream and downstream cell-gel composites based on the estimated input and output AI-2 concentrations from Fig. 2(b). That is, all fluidic process parameters (flow rates, dimensions, estimated cell densities, etc.) were fixed and we varied the synthesis/uptake rate of the transmitter and modulator cell populations from - 14 µM/s to 1 µM/s. In this way, the AI-2 concentrations were computed spanning the known AI-2 concentrations of 4.5 for transmitter cells, and AI-2 concentrations of 3.0, 5.8 or 1.07 µM for reporter, enhancer and reducer cells, respectively.

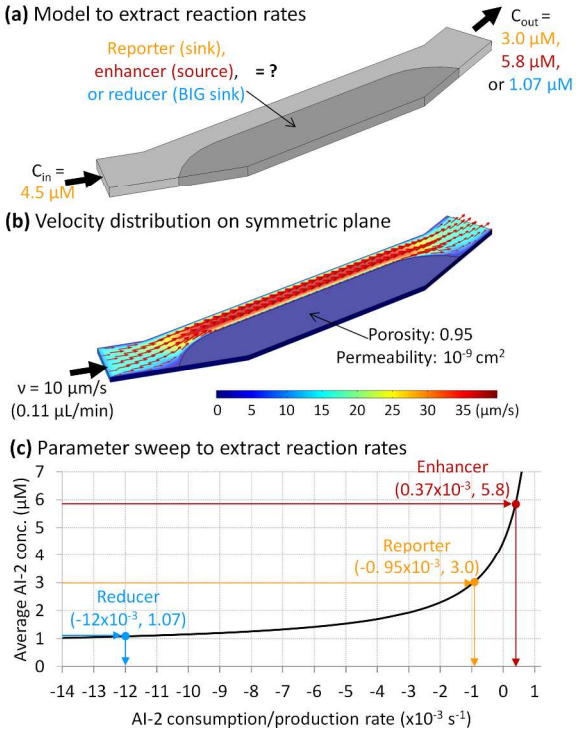

Fig. 3 Extracting reaction rates of the reporter, enhancer and reducer cells. (a) Numeric model with measured AI-2 concentrations of in-flow and out-flow. (b) Velocity distribution of the symmetric middle plane (120 µm from both channel ceiling and floor). (c) Parameter sweeping to extract reaction rates of reporter, enhancer and reducer cell-gel composites.

The resultant relationship between the upstream AI-2 output concentration and the reaction rate in the transmitter cell-gel composite was plotted in Fig. S2(b). These cells are exposed to fresh media and as noted in Fig. 1a, the fluid has two passes through the transmitter population. The net secretion rate is therefore consistent with the enhancer cells located in the downstream ecosystem. The reaction rate of transmitter cell-gel composite was estimated to be 0.405×10^{-3} s^{-1}, and the AI-2

distribution in the transmitter cell-gel composite was computed as shown in Fig. S2(c). The resultant relationship between the downstream AI-2 output concentration and the reaction rate in the downstream cell-gel composite was plotted as the black curve in Fig. 3(c). The reaction rates of the reporter, enhancer and reducer cells were determined to be - 0.95, 0.37 and - 12 × 10^{-3} s^{-1}, respectively. AI-2 distributions in the downstream cell-gel composites for the cases of reporter, enhancer and reducer cells are similarly shown in Fig. S4.

The net positive reaction rate for the enhancer cells was 0.37 μM/s, which means that more AI-2 had been produced by the enhancer cells and diffused into the flow passing the enhancer cell-gel composite than was otherwise taken up. The negative reaction rate of -0.95 × 10^{-3} s^{-1} means that the reporter cells had consumed a relatively high level of AI-2 diffusing from the nearby flow. The negative reaction rate of -12 × 10^{-3} s^{-1} of the reducer cells also suggests that they had consumed a significant amount of AI-2 diffusing from the nearby flow. As noted above, that the enhancer cells had a production rate an order of magnitude less than for transmitter cells was not unexpected. The AI-2 production rate is proportional to metabolic activity[36] and the transmitter cells, owing to the inlet of fresh media, have significantly higher metabolic activity. Also, we have noted previously that the net AI-2 production rate from BL21 cells (transmitters) is several fold higher than W3110 derivative LW5, which contains the fully expressed *Lsr* uptake transporter[37]. It is also possible that the second pass of media through these cells contributed to the net increase. If we assemble these factors, the net change is within our understanding.

In summary, simulations in COMSOL were used to elucidate the AI-2 reaction rates of the reporter, enhancer and consumer cells to be - 0.95, 0.37 and - 12 × 10^{-3} s^{-1}. The numeric results were computed based on the experimental results of the AI-2 concentrations of the collected effluent solutions. Importantly, they were consistent with previous reports[18, 22, 32].

D. Simulated AI-2 distributions in side-by-side modulator and reporter cell-gel composites

A significant goal of this cell-cell signalling simulation study was to investigate the effects of the modulator (enhancer and reducer) cell populations on the signalling between the transmitter and the reporter cell populations. We next quantified AI-2 distributions within the modulator and reporter cell-gel composites as shown in Fig. 4(a), where the modulator and reporter cell-gel composites were assembled side-by-side in the downstream microchannel. We assumed that the reaction rates of the reporter and modulator cells remained the same here as in the simulations of data in Fig.2. Note that the geometry of the reporter and modulator cell-gel composites in Fig. 4 was prorated to be half of that in Fig. 3. We also assumed the AI-2 concentration of the incoming flow remained constant at 4.5 μM. The modulator composite layer here represents three conditions: (1) an enhancer cell-gel composite, (2) a pure alginate hydrogel (control), or (3) a reducer cell-gel composite.

The simulation results in Fig. 4(b) show that AI-2 was uniformly distributed throughout the side-by-side cell-gel composites for all three cases. For the case of enhancer, the AI-2 levels in both the side-by-side enhancer and reporter cell-gel composites were over 4 μM. For the case of clear gel as the control, the AI-2 levels in both the side-by-side clear gel and reporter cell-gel composites were around 3 μM. For the case of reducer, on the other hand, the levels of AI-2 in both the side-by-side reducer and reporter cells were typically significantly below 1 μM.

E. Measured modulation of cell-cell communication with engineered cell communities

The experimental results of the modulation of cell-cell signalling with QS engineering cells are shown in Fig. 5. Fig. 5(a) shows the flux of signal molecules and the modulating cells assembled side-by-side with the reporting cells in four configurations: (1) clear alginate hydrogel without mediating cells (control), (2) with enhancer cells, (3) with reducer cells, or (4) with two layers of reducer cells sandwiching the reporter cells. The areas of the reporter regions in Fig. 5(a) for the aforementioned four cases were estimated to be 2.4 mm^2, 1.9 mm^2, 2.2 mm^2 and 2.3 mm^2, respectively, with an average of 2.2 ± 0.2 mm^2. The CT104 reporter cells were engineered so they were devoid of AI-2 production capability (*luxS*$^-$), but they can sense AI-2 and express red fluorescent protein DsRed in response. The enhancer and reducer cells do not produce fluorescent proteins. Signalling molecules were produced by transmitter cells (BL21) in an upstream microchannel and flowed at 0.11 μL/min (a 2-hour transport time) to the downstream channel. The cellular responses (fluorescence intensity of DsRed) of the reporting cells at time 18 hours are shown in Fig. 5(b); zoomed-in images are shown in Fig. 5(c).

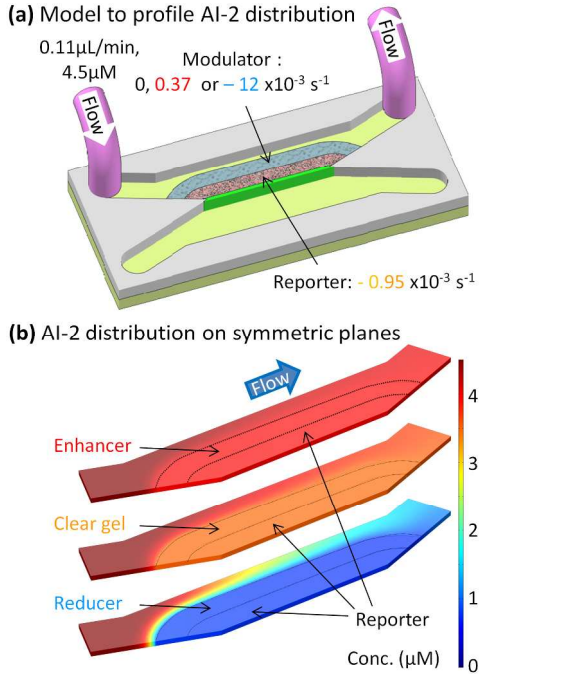

Fig. 4 Simulated AI-2 distribution in cell-gel composites. (a) Schematic with known in-flow parameters and extracted reaction rates. (b) AI-2 distribution on the middle planes of cell-gel composites in the cases of enhancer, clear gel (control) and one layer of reducer as modulator.

The results in Fig. 5 show that: (1) in the case of the control experiment where a clear gel was assembled along with the reporter cell-gel, the reporter cells at the edge of the reporter cell-gel composite displayed the highest fluorescence intensity,

presumably due to their access to both nutrients and AI-2. In addition, their ability to grow into the extra "empty" space in the adjacent gel may have enabled a more prominent response. We have no data to support the latter, however. Inside the reporter cell-gel composite margins, the fluorescence intensity was fairly high and uniformly distributed; (2) in the case of enhancer cells assembled along with the reporter cell-gel, the fluorescence intensity in the reporter cells was much higher than that for the case of the clear gel control. In this case, the fluorescence among the reporter cells was also fairly uniform and quite bright; (3) in the case of one layer of reducer cells assembled along with the reporter cell-gel, the fluorescence intensity of the reporter cells is minimal compared to that for both the cases of clear gel and enhancer cells; and finally, (4) in the case of two layers of reducer cells sandwiching the reporter cell-gel, the fluorescence intensity in the reporter cells is not detectible with our experimental setting. We note that the AI-2 signal transduction process of CT104 cells is triggered at concentrations near or above 1 μM[22], which is consistent with the simulations in Fig. 4.

These results clearly demonstrated for the first time, cell-cell signalling in remotely connected transmitter and reporter cell populations even in the case of the control experiment. The results further demonstrate that the enhancer cell population had functioned as a signalling enhancer via providing more AI-2 to increase the cellular response in the adjacent reporter cells. The reducer cells efficiently consumed the majority of AI-2 before the signal molecules reached the reporter cells and resulted in the signalling quenching. In other words, both the enhancer and reducer cells had successfully modulated the population-to-population communication between the remotely connected transmitter and reporter cells.

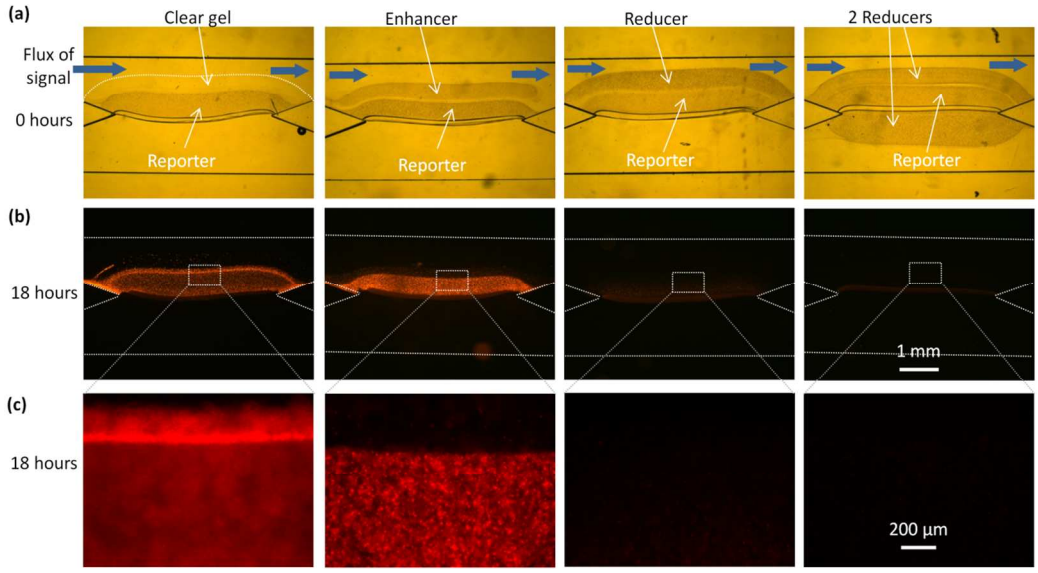

Fig. 5 Modulating cell-cell signaling with QS engineering cells. **(a)** Flux of signal molecules and the corresponding configurations of mediating cells assembled around reporting cells. **(b)** Fluorescent micrographs showing the red fluorescent proteins (DsRed) in reporting cells at 18 hours. **(c)** Zoom-in views of one set of fluorescent micrographs of reporting cells at 8 hours.

F. Measured time-course cellular response and estimated time-course AI-2

We have shown for the first time, molecular signals emanating from model bacterial cell populations can be transmitted to reporter populations located ~2 hr downstream. This is consistent with flow profiles of the human GI tract. We have further demonstrated the viability of signal modulating cell populations and the effects on cell signalling in distant locales. These advances will enable more comprehensive human-on-a-chip systems for studies of drug discovery and delivery. In order to more quantitatively develop these micro-hydrodynamic human organ systems, co-development of pharmacokinetic and pharmacodynamics (PK/PD) models have been called for[38]. In our case, real time cellular responses and cell growth were monitored via phase contrast and fluorescence microscopy (Fig. 6).

Cell optical density (OD) in Fig. 6(a) shows a typical cell growth curve (green curve, left axis) as calculated from transmitted light images after a background subtraction. The green dots are the measured OD, while the green line is an exponential best fit curve with a time constant of 1.6 hours with the following space-constrained logistic growth equation (i):

$$OD = OD_{max}\,(1 - \mathrm{e}^{-t/\delta_{od}}) \qquad \text{eq. (i)}$$

where OD_{max} is the maximum OD, and δ_{od} is the time constant. The accumulated cell OD represents the net increase of cell density over time. We note the cell growth tendency for all the cells in the cell-gel composites in the microfluidic channels similarly followed the growth curve shown in Fig. 6(a). Next, the area-averaged fluorescence intensity of the reporter cells was recorded every hour for a time period of 18 hours and is shown as a collective set (Fig. 6(a), right axis). We fit each experimental condition to the following equation (ii):

$$I = I_{max}\,(1 - \mathrm{e}^{-t/\delta_i}) \qquad \text{eq. (ii)}$$

where I_{max} is the maximum fluorescence intensity, and δ_i is the time constant. These model calculations are represented by dashed lines. In the case of the control experiment, the fluorescence intensity of the reporter cells (orange dots and

dashed curve) increased with time, following equation (ii) and reached a fairly high level (~ 40 a.u.); the time constant was determined to be 1.75 hours. In the case of enhancer cells, the fluorescence intensity of the reporter cells (red dots and dashed curve) levelled off at a much higher level almost 2X of that of the control; the time constant was again ~ 1.75 hours. In the case of one layer of reducer cells (blue dots and dashed curve), the fluorescence intensity of the reporter cells was only ¼ that of the control; the apparent time constant was ~ 5 hours. Finally, in the case of two layers of reducer cells sandwiching the reporter cell-gel (black dots and dashed curve), the fluorescence intensity in the reporter cells was not detectable using our experimental setting; the time constant could not be defined.

The time delays pertaining to the appearance of the fluorescence signals are informative. For the case of enhancer cells where downstream AI-2 is immediately available to the reporter cells, the time delay was about 4 hours, which is presumably the time lag for fluorescent protein expression. This is consistent with our previous report using similar cells, but not in cell-gel composites[39]. For the cases of clear gel (control) and reducer cells where AI-2 was only available after a 2-hour delay corresponding to the transport time from the upstream microchannel, the observed time delay was about 6 hours, which is also the sum of both the transport time and fluorescent protein expression time lag. These time delays are indicated between the upper and lower panels of Fig. 6.

Finally, we estimated the amount of AI-2 available to the reporter cells in the reporter cell-gel composites over time. As a simplification, we assumed that the AI-2 production and consumption rates remained constant as previously calculated for each cell population over the 10 hour time period (4.05×10^{-3} s^{-1}, 0.37×10^{-3} s^{-1} and - 12×10^{-3} s^{-1} for transmitter, enhancer and reducer cells, respectively). Further, as our goal was to estimate the accumulated AI-2 available to reporter cells, we also assumed that the consumption rate of reporter cells is zero. As such, the total AI-2 production from both the transmitter and enhancer cells should be proportional to the cell OD over time following the curve in Fig. 6(a) with a time constant of 1.6 hours. Further, for the AI-2 secreted from the transmitter cells (upstream), the available AI-2 will have a 2 hour lag. Therefore, the available AI-2 over time within the reporter cell-gel composites could be simulated for the three cases: (1) with enhancer cells; (2) with clear gel (control); and (3) with one layer of reducer cells. Our simulated time-course curves for AI-2 concentration are shown in Fig. 6(b) (left axis). The ratio of AI-2 concentration to the optical density of reporter cells is similarly shown (Fig. 6(b), right axis) The simulation results show that in the case of enhancer cells, AI-2 (red solid curve) was immediately available for the reporter cells for the first two hours, after which point the available AI-2 thereafter was the combination of that synthesized by enhancer cells and that transported from upstream channel. We note the level available to the cells rapidly reached ~ 0.8 μM in the cell-gel composite, which is sufficient to trigger gene expression in CT104 cells[25]. Contrarily, in the cases of the clear gel (orange solid curve) and the reducer cells (blue solid curve), AI-2 was only available from the transmitter cells and therefore a 2-hour delay was incurred. Therefore, the total amount of AI-2 was lower than in the case of enhancer cells. In the case of one layer of reducer cells, there was also a 2-hour delay for AI-2 to be available for reporting cells, and the total amount of AI-2 was minimal compared to that in the cases of enhancer cells and clear gel. These data support the hypothesis that ~0.3 μM AI-2 is sufficient to initiate a QS response in these cells.

Notably, our estimation of available AI-2 to the reporter cells was performed using several broad assumptions, including constant reaction rates over time and space. Even with these simplifications, we note that the estimated available AI-2 in Fig. 6(a) agrees fairly well with the experimentally measured fluorescence intensity in all the three cases of enhancer, clear gel and reducer cells, and with our previous reports[19, 25, 39].

In summary, we have employed numerical simulation to approximate the available AI-2 to the reporting cells. The simulations and the experiments were in good agreement, particularly within the dynamic period of the first few hours. The experimental measurements of the fluorescence intensity demonstrate, for the first time, real time access to signalling events in a distributed microfluidic network. Importantly, the characteristic lag associated with laminar flow in microfluidic channels enabled strong predictive power. Both the simulation and experimental studies have showed that distally placed modulator cell populations effectively "tune" the amount of signal molecule AI-2 transferred between the transmitter and reporter cells.

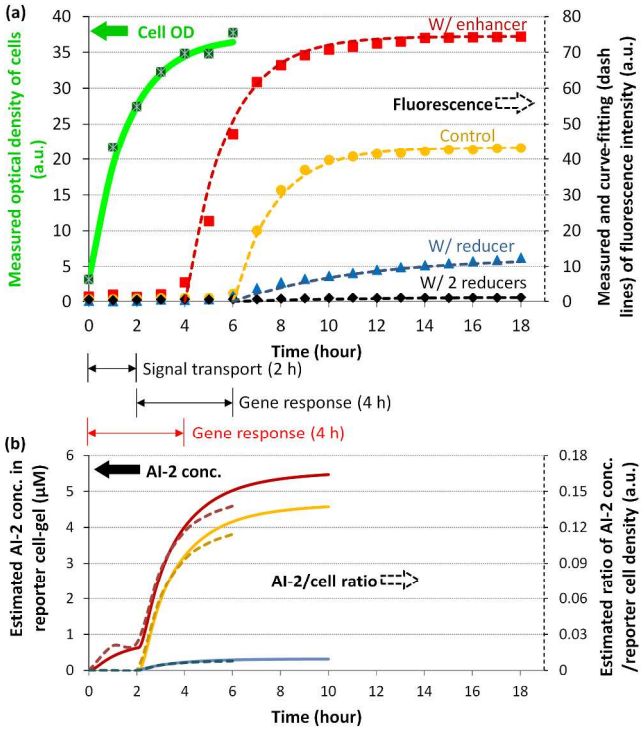

Fig. 6 Time-course cellular response of reporting cells with the corresponding simulated AI-2 concentration in the reporter cell-gel composites. **(a, left axis)** Typical cell growth curve based on optical density measurement of cells. **(a, right axis)** Time-course fluorescence intensity of the reporter cells over 18 hours for the cases of enhancer, clear gel (control), one layer of reducer, and two layers of reducer as modulators. **(b, left axis, solid)** Estimated AI-2 concentration within the reporter cell-gel composites for the beginning 6 hours for the cases of enhancer, clear gel (control) and one layer of reducer as modulator. **(right axis, dotted)** Ratio of the estimated AI-2 concentration to the measured optical density of reporter cells.

Conclusions

Using biofabrication methods for the assembly of engineered cell communities, we have shown the transport of signalling molecules flowing within cascaded microfluidic channels, and the active enhancement or elimination of the signalling between two communicating cell populations. Both experimental assays and numerical simulations were employed to quantitatively evaluate the synthesis and consumption dynamics of signalling molecules and cell responses. Our study suggests there is great potential for investigating more complex *in vitro* models of the human GI tract and other connective organs, where signals emanating from one cell population are transmitted and acted upon by other cell populations. Importantly, our biofabrication methods, which employ stimuli responsive biopolymers chitosan and alginate for the rapid and gentle assembly of cells, enable their interrogation in near real time and with little mechanical input. Our cells in this case are bacteria whose response to high cell density is normally a well-orchestrated QS response. In our case, we can control the QS response by flow and in this specific instance, we demonstrate that "modulator" cells placed in the device are able to modulate the signal so that the "response" cells can accurately report on the prevailing conditions *in situ*. We recognize this bacteria-bacteria system is a gross simplification of the GI tract. This is the first instance where an *in vitro* model dynamically reports bacteria-bacteria signalling among distant populations. Moreover, the methods developed are simple and robust so that complex synthetic eco-systems can be constructed by the inclusion of different cell populations (epithelial cells, other bacteria) and manipulating effector molecules (glucose, hormones, ions) with geometrical and temporal guidance.

Acknowledgements

This work was supported by the Burns Junior Faculty Fellowship in the College of Engineering at the Catholic University of America, the Robert W. Deutsch Foundation, the National Science Foundation (CBET 1264509 & 1160005) and the Defense Threat Reduction Agency (HDTRA1-13-1-0037). We acknowledge the support of the Maryland NanoCenter and its FabLab.

Notes

[a] *Department of Mechanical Engineering, Catholic University of America, Washington, DC 20064, USA*
[b] *Institute for Bioscience and Biotechnology Research (IBBR), University of Maryland, College Park, MD 20742, USA. Fax: 01 301 405-9953; Tel: 01 301 405-4321; E-mail: bentley@umd.edu*
[c] *Fischell Department of Bioengineering, University of Maryland College Park, MD 20742, USA*
[d] *Institute for Systems Research (ISR), University of Maryland College Park, MD 20742, USA*
[e] *Department of Materials Science and Engineering, University of Maryland, College Park, MD 20742, USA.*

† Electronic Supplementary Information (ESI) available: [details of any supplementary information available should be included here]. See DOI: 10.1039/b000000x/

‡ Footnotes should appear here. These might include comments relevant to but not central to the matter under discussion, limited experimental and spectral data, and crystallographic data.

References

1. R. E. Ley, *Current opinion in gastroenterology*, 2010, 26, 5-11.
2. D. Kelly, S. Conway and R. Aminov, *Trends in immunology*, 2005, 26, 326-333.
3. F. Guarner and J.-R. Malagelada, *The Lancet*, 2003, 361, 512-519.
4. L. Gravitz, *Nature*, 2012, 485, S12-S13.
5. F. Backhed, R. E. Ley, J. L. Sonnenburg, D. A. Peterson and J. I. Gordon, *Science*, 2005, 307, 1915-1920.
6. N. M. Koropatkin, E. A. Cameron and E. C. Martens, *Nat. Rev. Microbiol.*, 2012, 10, 323-335.
7. A. W. Walker, J. D. Sanderson, C. Churcher, G. C. Parkes, B. N. Hudspith, N. Rayment, J. Brostoff, J. Parkhill, G. Dougan and L. Petrovska, *BMC Microbiol.*, 2011, 11.
8. J. Gong and C. B. Yang, *Food Res. Int.*, 2012, 48, 916-929.
9. P. Van den Abbeele, C. Belzer, M. Goossens, M. Kleerebezem, W. M. De Vos, O. Thas, R. De Weirdt, F. M. Kerckhof and T. Van de Wiele, *Isme J.*, 2013, 7, 949-961.
10. M. Rajilić-Stojanović, H. G. H. J. Heilig, D. Molenaar, K. Kajander, A. Surakka, H. Smidt and W. M. De Vos, *Environmental Microbiology*, 2009, 11, 1736-1751.
11. A. Kumari, P. Pasini, S. K. Deo, D. Flomenhoft, H. Shashidhar and S. Daunert, *Analytical Chemistry*, 2006, 78, 7603-7609.
12. N. Raut, P. Pasini and S. Daunert, *Anal. Chem.*, 2013, 85, 9604-9609.
13. K. Nagy, O. Sipos, E. Gombai, A. Kerenyi, S. Valkai, P. Ormos and P. Galajda, *Chem. Biochem. Eng. Q.*, 2014, 28, 225-231.
14. S. Park, X. Q. Hong, W. S. Choi and T. Kim, *Lab Chip*, 2012, 12, 3914-3922.
15. H. J. Kim, J. Q. Boedicker, J. W. Choi and R. F. Ismagilov, *Proc. Natl. Acad. Sci. U. S. A.*, 2008, 105, 18188-18193.
16. H. H. Wang, M. T. Mee and G. M. Church, *Synthetic Biology: Tools and Applications*, 2013, DOI: 10.1016/b978-0-12-394430-6.00017-0, 317-325.
17. V. Roy, M. T. Meyer, J. A. I. Smith, S. Gamby, H. O. Sintim, R. Ghodssi and W. E. Bentley, *Appl. Microbiol. Biotechnol.*, 2013, 97, 2627-2638.
18. J. F. Betz, Y. Cheng, C. Y. Tsao, A. Zargar, H. C. Wu, X. Luo, G. F. Payne, W. E. Bentley and G. W. Rubloff, *Lab Chip*, 2013, 13, 1854-1858.
19. X. Luo, H.-C. Wu, C.-Y. Tsao, Y. Cheng, J. Betz, G. F. Payne, G. W. Rubloff and W. E. Bentley, *Biomaterials*, 2012, 33, 5136-5143.
20. Y. Cheng, X. Luo, C. Y. Tsao, H. C. Wu, J. Betz, G. F. Payne, W. E. Bentley and G. W. Rubloff, *Lab Chip*, 2011, 11, 2316-2318.
21. S. J. Hur, B. O. Lim, E. A. Decker and D. J. McClements, *Food Chemistry*, 2011, 125, 1-12.
22. L.-Q. Wu, A. P. Gadre, H. Yi, M. J. Kastantin, G. W. Rubloff, W. E. Bentley, G. F. Payne and R. Ghodssi, *Langmuir*, 2002, 18, 8620-8625.
23. X. L. Luo, D. L. Berlin, J. Betz, G. F. Payne, W. E. Bentley and G. W. Rubloff, *Lab Chip*, 2010, 10, 59-65.
24. C. Y. Tsao, S. Hooshangi, H. C. Wu, J. J. Valdes and W. E. Bentley, *Metabolic Engineering*, 2010, 12, 291-297.
25. H. C. Wu, C. Y. Tsao, D. N. Quan, Y. Cheng, M. D. Servinsky, K. K. Carter, K. J. Jee, J. L. Terrell, A. Zargar, G. W. Rubloff, G. F. Payne, J. J. Valdes and W. E. Bentley, *Mol. Syst. Biol.*, 2013, 9.

26. L. Wang, Y. Hashimoto, C. Y. Tsao, J. J. Valdes and W. E. Bentley, *Journal of Bacteriology*, 2005, 187, 2066-2076.
27. B. L. Bassler, M. Wright and M. R. Silverman, *Molecular Microbiology*, 1994, 13, 273-286.
28. Ü. Mehmetoğlu and M. Hacimusalar, in *Recent Advances in Biotechnology*, eds. F. Vardar-Sukan and Ş. S. Sukan, Springer Netherlands, 1992, vol. 210, ch. 20, pp. 383-388.
29. S. Partap, A. Muthutantri, I. U. Rehman, G. R. Davis and J. A. Darr, *Journal of Materials Science*, 2007, 42, 3502-3507.
30. C. M. Hwang, S. Sant, M. Masaeli, N. N. Kachouie, B. Zamanian, S.-H. Lee and A. Khademhosseini, *Biofabrication*, 2010, 2.
31. J. L. Terrell, T. Gordonov, Y. Cheng, H. C. Wu, D. Sampey, X. Luo, C. Y. Tsao, R. Ghodssi, G. W. Rubloff, G. F. Payne and W. E. Bentley, *Biotechnology journal*, 2012, 7, 428-439.
32. D. N. Quan and W. E. Bentley, *PLoS computational biology*, 2012, 8, e1002637.
33. G. Q. Hu, Y. L. Gao and D. Q. Li, *Biosens. Bioelectron.*, 2007, 22, 1403-1409.
34. T. Gordonov, E. Kim, Y. Cheng, H. Ben-Yoav, R. Ghodssi, G. Rubloff, J. J. Yin, G. F. Payne and W. E. Bentley, *Nature nanotechnology*, 2014, 9, 605-610.
35. K. B. Xavier and B. L. Bassler, *Nature*, 2005, 437, 750-753.
36. M. P. DeLisa, J. J. Valdes and W. E. Bentley, *Journal of Bacteriology*, 2001, 183, 2918-2928.
37. C.-Y. Tsao, S. Hooshangi, H.-C. Wu, J. J. Valdes and W. E. Bentley, *Metabolic Engineering*, 2010, 12, 291-297.
38. J. H. Sung, C. Kam and M. L. Shuler, *Lab Chip*, 2010, 10, 446-455.
39. R. Fernandes, X. L. Luo, C. Y. Tsao, G. F. Payne, R. Ghodssi, G. W. Rubloff and W. E. Bentley, *Lab Chip*, 2010, 10, 1128-1134.